Structure-Property Relationships in Solvent Free Adhesives Derived from Castor Oil

Harshal D. Santan[a,†,*], Craig James[b,#], Emiliano Fratini[b], Inmaculada Martínez[a], Concepción Valencia[a], María. C. Sánchez[a], and José M. Franco[a]

[a] Departamento de Ingeniería Química, Pro2TecS, Facultad de Ciencias Experimentales, Universidad de Huelva, Campus de El Carmen, Huelva 21071, Spain.

[b] Department of Chemistry "Ugo Schiff" & CSGI, University of Florence, via della Lastruccia, 3, Sesto Fiorentino 50019, Florence, Italy.

† Present Address: Department of Chemistry "Ugo Schiff" & CSGI, University of Florence, via della Lastruccia, 3, Sesto Fiorentino 50019, Florence, Italy.

Present Address: School of Chemistry, Cardiff University, Park Place, Cardiff, CF10 3AT, UK.

* Corresponding author E-mail address: santan@csgi.unifi.it (H.D. Santan)

Abstract

A method to prepare solvent free castor oil (CO) based polyurethane (PU) adhesives with different ratios of CO and hexamethylene diisocyanate (HMDI) has been developed and the relationships between the microstructure and mechanical properties investigated. Solvent free castor oil-based PU adhesives were synthetized by promoting the reaction between castor oil and HMDI, at room conditions, and by varying the CO/HMDI weight ratio in the range 1:0.032 - 1:0.32 wt%. The curing of these adhesives did not require any external stimuli such as heat or irradiation treatment and once cured at room temperature they were stable up to 140 °C and water-resistant. A multi-technique approach was used to characterize so-obtained adhesives. The adhesion energy in metal-metal contact was evaluated as a function of the debonding velocity (V_d) through tack experiments. The mechanical properties were influenced by the -NCO/-OH ratio, which varies the crosslinking density in the adhesives. Moreover, the structure–mechanical property relationship was explored and the inter-

correlation between the storage modulus (G'), adhesion energy (E_{ad}) and correlation length (ξ) detailed, with both G', E_{ad} increasing while ξ decreased. These solvent-free bio-based adhesives showed capability to adhere different substrates such as wood, paper, textile, and metal, which makes them promising candidates in different industrial and commercial applications.

Keywords: Adhesive; Rheology; Castor Oil; Polyurethane; Structure-Property Relationships.

1. Introduction

Polyurethanes (PU) derived from different sources have been used in many industrial applications as adhesives, coatings, paints, lubricants, thermoplastic elastomers, and foams (Ebnesajjad and Landrock, 2015; Engels et al., 2013; Lambuth, 1989). The suitability in such a wide range of applications is due in part to the potential of modifying the physical and chemical properties of the basic building blocks (Frisch, 2002). In recent years, the preparation of such polyurethanes from renewable resources and the replacement of synthetic polymers have gained the attention of researchers across the world. Naturally occurring vegetable oils are currently the prominent focus of both academic and industrial research and development into renewable resources (Donnelly et al., 1991; Zhang et al., 2015). During the past few decades, castor oil has been widely investigated as a potential source material for the preparation of polyurethanes. It is a naturally occurring, environmental friendly and inexpensive material that contains secondary hydroxyl groups in the predominant ricinoleic fatty acid (80–95 % in the fatty acid profile) that are available for functionalization. Adhesives based on naturally sourced materials have been developed in recent years to replace traditional formulations and overcome disadvantages such as toxicity, use of organic solvents, material cost, and degradability (Donnelly et al., 1991; Zuber et al., 2015) Such volatile, solvent-free adhesives can be produced by using natural resources at low prices whilst being biodegradable and are therefore highly sought after when compared to those produced from petrochemical derived products. Polyurethanes based on biodegradable polyols (Howard, 2002), and particularly biopolymers containing urethane linkages (Gallego et al., 2015; Ratajska and Boryniec, 1998), are considered largely biodegradable materials. In

recent years, some polyurethane prepolymers based on castor oil and isocyanates were synthesized and characterized as adhesives and coatings (Gurunathan et al., 2015; Silva et al., 2010; Somani et al., 2004, 2003; Tenorio-Alfonso et al., 2018). However, the basic understanding and elucidation of the structural-mechanical properties and adhesiveness by varying the isocyanate concentration of such materials have not been investigated in great detail. Basically, these types of prepolymers are reactive products containing terminal isocyanate groups (–NCO) able to interact with another polymer containing active hydroxyl group (–OH) known as polyols or polyamines. This reaction leads to the formation of new polyurethane bonds. There are several factors such as composition of polyol and isocyanates, reaction temperature, and size of the isocyanate compounds which significantly affects the final physical and chemical properties of polyurethanes (Borrero-López et al., 2017; Gallego et al., 2014). The use of vegetable oils in combination with diisocyanate crosslinkers may provide a different degree of physical interactions (intra and inter molecular) which may also contribute to the final physical properties of polyurethane such as adhesiveness, thermal stability, curing time, etc. However, the micro- and molecular structure of these materials is a key element to understand their effectiveness as adhesives. Therefore, it is necessary to comprehend the rationale controlling the structure and then the final properties so to detail the microstructure-mechanical properties relationship in such adhesives derived from natural resources. In this study, model adhesive formulations based on castor oil, as a source of polyols, and HMDI, as crosslinker, were prepared and fully characterized to detail the effect of the crosslinking density on the final microstructure and adhesiveness. The aim of this investigation was to disclose the relationship between the structure and functional properties of such complex systems.

2. Materials and Methods

2.1 *Materials*:

Castor oil (211 cSt at 40 °C, Guinama, Spain) was used as received without any purification. 1,6-hexamethylene diisocyanate (HMDI, purum grade, 98.0 %), triethylamine (≥ 99.5 %), and all other solvents were purchased from Sigma-Aldrich and used without further purification.

2.2 *Preparation of adhesives*:

The adhesives were prepared by means of a simple methodology to crosslink the castor oil molecules with HMDI under mild reaction conditions. For example, the adhesive CO-75 was prepared as follows: first, 75.66 g of castor oil was dissolved in toluene (35 ml) at room temperature followed by agitation for 20 minutes to form a homogeneous solution. Triethylamine was then added in excess (6.35 ml) to the reaction mixture followed by drop wise addition of 24.34 g of HMDI. After complete addition of HMDI, the mixture was stirred for 2 days at room temperature. The toluene from the crude product was removed under vacuum by rota-evaporator at 65-70 °C for 15-20 minutes to obtain a viscous liquid. The curing of all adhesives was performed by keeping the samples in open air at room conditions (temperature: 25ºC ±2ºC; relative humidity: 63% ± 3 %) for the time required for the complete reaction of all free isocyanates. Generally, the curing time was dependent on the amount of HMDI added in the composition and was ranging in between 24-48 hours (data not shown). The same experimental set-up was used to prepare all CO-based adhesives with the different CO/HMDI weight ratios studied. Table 1 includes the different CO/HMDI weight ratios and the corresponding –NCO/–OH mole ratios according to the CO fatty acid profile previously reported (Quinchia et al., 2010), as well as the codes applied for each sample. Some of the adhesives prepared are shown in Figure S1 of the Supporting Information (ESI).

2.3 Measurements

2.3.1 *ATR-FTIR measurements*:

Fourier transformation infrared spectroscopy (FTIR) was used was used to determine the functional groups of synthesized adhesives. The spectra were obtained by using FTIR-4200 spectrometer

(JASCO) with the wavenumber range from 400 to 4000 cm^{-1}, at a resolution of 4 cm^{-1}, in transmission mode. Samples were placed directly on an attenuated total reflectance (ATR) accessory provided with monolithic diamond crystal.

2.3.2 *Thermogravimetric analysis (TGA)*:

Measurements of thermal stability and degradation were carried out by means of TGA. The experiments were carried out under constant nitrogen purging using a model Q-50 (TA Instruments, DE, USA) thermogravimetric analyser. Typically, ~10 mg of sample were placed on a platinum pan and heated from 30 °C to 600 °C, at a heating rate of 10 °C/min.

2.3.3 *Rheology*:

The rheological measurements were investigated with a controlled-stress MARS rheometer (Thermo Haake, Germany) using parallel plate-plate geometry (35 mm). Small-amplitude oscillatory shear (SAOS) measurements inside the liner viscoelastic range were carried out after removal of toluene i.e. before curing (BC) and after curing (AC) of the adhesives. Both viscous (before curing) and solid-like (after curing) samples were placed directly between the plate-plate geometry prior to gap adjustment. Frequency-sweep experiments were performed in the range of 0.01-20 Hz. Initial stress-sweep tests were carried out to determine the linear viscoelasticity range for each sample. All the experiments were performed at 25 °C.

2.3.4 *Probe tack experiments*:

The tack tests (adhesion tests) were carried out in a Shimadzu AG-IS Universal Testing Machine (Japan), using a 500 N load cell and smooth steel plate-plate geometries (35 mm), at 25 °C. Tests were performed using two initial gaps (0.5 and 0.1 mm) between the plates and debonding speeds (V_d) of 1 and 5 mm/s for each gap. The contact time between adhesive and surface was always 1 minute for all

probe tack measurements performed just to ensure a good contact with the plate surface. The required normal force for debonding was measured as a function of time.

2.3.5 *Small Angle X-ray Scattering (SAXS)*:

SAXS measurements were performed using a HECUS, S3-MICRO Kratky-type camera equipped with a position sensitive, 50M OED detector comprising of 1024 channels, 54 μm in width. An ultra-brilliant point microfocus X-ray source (GENIX-Fox 3D, Xenocs, Grenoble) provided Cu Kα radiation with a wavelength, λ, of 1.542 Å at a maximum power of 50 W. A sample-to-detector distance of 281 mm allowed for a measurable q-range between 0.01 and 0.54 $Å^{-1}$ (where q, the scattering vector, is given by $q = 4\pi/\lambda \sin\theta$, and 2θ is the scattering angle). The S3-MICRO camera was calibrated using silver behenate (d = 58.38 Å)(Raftery and Gilles, 1995) and kept under vacuum to reduce scattering from air. Samples were placed into demountable cells with Kapton film windows giving a sample thickness of 1 mm. Measurements were performed at a temperature of 25 °C and controlled by a Peltier element with an accuracy of 0.1 °C. Raw scattering data were corrected for the scattering of the cell and unreacted pure castor oil using the relative transmission factor.

2.3.6 *Scanning electron microscopy (SEM):*

The surface morphology of cured adhesives was analysed by SEM observations, using a JEOL, JSM-5410 scanning electronic microscope. Typically, the solid adhesive samples were cut in approximately 0.5 cm^2 slices and mounted onto metal stub with double sided carbon tape. The sample was then coated with a thin layer of gold using an automated sputter coater.

3. Results and discussion

3.1 FT-IR Spectrum of the adhesives

The Fourier transform infrared spectra of pure castor oil and adhesive samples CO-97 to CO-75 are shown in Figure 1. Basically, castor oil shows a broad band in the range 3350-3600 cm^{-1} corresponding to hydroxyl groups, and an intense characteristic peak at 1740 cm^{-1} corresponding to the stretching vibration of C=O carbonyl bond of triglyceride ester. As the spectra were measured after curing of adhesives, the typical absorption peak of free isocyanate (-N-C=O) groups, easily traceable around 2270 cm^{-1}, was hard to see in the spectra of cured adhesives, which confirmed that all isocyanate groups were reacted quantitatively during the synthesis and curing process. Other absorption peaks also confirm the reaction between free hydroxyl groups of CO and HMDI. Thus, the urethane bond formation can be seen by the absorption peaks at 1530-1545 cm^{-1} due to R-HN-C=O amide II vibrations and 1690-1700 cm^{-1} due to -C=O stretching in the urethane linkage. Interestingly, the absorption at 3350-3600 cm^{-1} decreased along with slight shift and the absorption at 3360-3380 cm^{-1} increased due to –NH stretching. This indicates the significant reduction of free –OH groups, which took part in formation of new urethane groups. Moreover, the absorption at 1530-1545 cm^{-1}, characteristic of the –C-N- bond in the urethane group correctly increases with the amount of HMDI in the composition. Additionally, the strong absorptions at 3032-3095 cm^{-1} and 1505-1510 cm^{-1}, which correspond to aromatic C-H and C-C stretching respectively from toluene, was not found in all the samples measured. Hence, it may be inferred that the toluene was removed almost completely from the final product.

3.2 Thermal Analysis

The change in the chemical structure was also determined by TGA analysis which gives an estimation of the thermal stability and degradation of the adhesives as a function of the composition. The thermal degradation of PU adhesives is generally dependent on the number of urethane linkages in the system and therefore relates to the amount of HMDI added in the composition (Borrero-López et al., 2017). The thermal degradation in such system starts with the degradation of urethane bonds, which transform into isocyanate and alcohol species. Further heating at higher temperatures may form

primary and secondary amines and CO_2 with a greater weight loss (Simon et al., 1988). As shown in Figure 2, thermograms of PU adhesives show different patterns of degradation but generally consist of one main degradation step in line with difference in composition. The temperature at which the major weight loss was initiated, T_{onset}, decreases from 364 to 323 °C when increasing the amount of HMDI in the composition from CO-97 to CO-75 (see Table S2 in ESI). The thermal stability of the inspected samples had the very same trend. This is a clear indication that increasing the number of urethane bonds, the system tends to be more easily degraded; a characteristic that actually correlates with the theoretical model of PU-based materials (Gallego et al., 2014) and testify that the urethane bonds destabilize the molecular structure of the adhesive. The pattern of degradation also changes from single step (eliminating the initial mass loss at 60–90 °C due to moisture) degradation for CO to two or three overlapped degradation steps passing from CO-97 to CO-75. The temperature at which the maximum degradation rate occurred for pure CO was 390 °C, with a total degradation temperature range of 360-480 °C (see Figure 2B). The degradation pattern and weight loss temperature ranges of CO-97 and CO-95 samples are more similar to CO due to the small degree of functionalization, although the overall thermal stability (T_{onset}) was found to be comparable. However, the thermal degradation of CO-95 showed a slightly different pattern with a more extended mass loss temperature range of 395 – 470 °C. In the samples CO-86 and CO-75, the thermal stability was remarkably reduced due to the increase in the number of polyurethane segments, which are degraded at lower temperatures compared to pure CO (Gallego et al., 2015; Mythili et al., 2004). The derivative thermograms (see Figure 2B) of CO-86 and CO-75 reveal the existence of three different degradation stages that are not evident in the rest of the compositions. However, the maximum degradation rate temperature (T_{max}) is slightly decreased compared with the rest of series (see Table S1 in ESI). Overall, the TGA shows the effect of –NCO/–OH ratio on the thermal stability of the adhesives due to changes in both the chemical composition and polymer network formed during crosslinking.

3.3 Rheological measurements

The rheological measurements were performed to determine the effect of CO/HMDI weight ratio on the mechanical properties before and after the curing process. The effect of -NCO/-OH ratio on the storage modulus (G') after curing is presented in Figure 3 by controlled-stress amplitude sweep measurements inside the linear viscoelastic range. As expected, the lowest G' values (~4 Pa) were found for the adhesive with the lowest CO/HMDI weight ratio, which also exhibited a limited viscoelastic range (up to around 2 Pa). A further increase in the isocyanate index from 0.36 to 1.43 significantly increased the storage modulus from 50 Pa to 57 kPa. In all these cases, the storage modulus also showed an extended linear viscoelasticity range as well as a plateau region within the investigated frequency range (see Figure 4B) indicating a constant gel-like behaviour after curing. However, it is also to be noted that after cuing, significant decrease in the frequency dependent viscoelastic behaviour was observed (Figure 4B). This agrees with the fact that there are no free isocyanate groups left in the adhesive, which could further lead to the formation of new urethane bonds (network points) and hence, responsible to increase the storage modulus. For lower concentrations of HMDI (CO-97, CO-95 and CO-92), even after curing, the loss modulus was always higher than storage modulus within the given frequency range (0.01-20 Hz), which is predominately due to the formation of partial crosslinking in these adhesives. To illustrate more specifically the effect of the evolving chemical structure on viscoelastic properties, amplitude sweep test before and after curing of the adhesives were performed at 25 °C. An example of this measure is shown in Figure 4A. Before curing, the loss modulus, G" (~41 Pa), of sample CO-75 was higher than the storage modulus, G' (~2 Pa), by one order of magnitude. However, during the curing process additional urethane-bond network points are formed from the reaction between available –NCO groups and –OH groups located in the fatty acid chain: as a result, the rigidity of the chemical structure increases. Therefore, G' increased up to 57 kPa, being higher than the G" value (~13 kPa). The dramatic changes in the viscoelastic properties of these samples are attributed to the formation of physical entanglements and chemical crosslinking during the curing process. The same analysis can be inferred from the mechanical spectra obtained in frequency sweep measurements (Figure 4B). The typical terminal

region of the spectrum, corresponding to a liquid-like behaviour ($G'' > G'$) and a tendency to reach a crossover point at high frequencies, was clear for all adhesives before curing. For additives containing more than 7 wt% HMDI, the above-mentioned plateau region ($G' > G''$) was noticed after curing. Overall, rheological measurements are very sensitive to the changes in chemical structure that occur during the curing process.

3.4 Probe-Tack Test

Besides SAOS measurements, the adhesiveness or stickiness was investigated by means of probe tack tests. It was assumed that the tack test could complement the knowledge of the viscoelastic properties of these adhesives. In particular, it is interesting to evaluate how the change in the viscoelastic properties can affect the tacking response of these adhesives. To investigate the effect of extensional strain rate on the adhesives strength, tack tests were performed using two different initial gaps (0.5 and 0.1 mm) and applying two different debonding speeds (1 and 5 mm/s). The adhesives were placed in between two parallel plate-plate geometries with fixed gap and the contact of plate and adhesive was maintained for 1 min before applying the different debonding speeds. Generally, the failure in adhesiveness was initiated by two main mechanisms. The first mechanism is through interfacial cavitation. It is typical for adhesives with low adhesive strength, and in this case, is evident for CO-97, CO-95, and CO-92. The second mechanism was through fibrous cavitation as shown by CO-86 and CO-75 which gave much higher adhesion strengths (Verdier and Piau, 2003). The normal force (F), time (t), and displacement (d) values were directly obtained from the probe tack test. Moreover, the normal stress (σ) *versus* strain (ϵ) curves were calculated starting from the values of initial adhesive thickness (h_0) and the initial contact area (A_o) as shown in Equations 1 and 2:

$$\sigma = \frac{F(t)}{Ao} \quad (1)$$

$$\epsilon = \frac{[d(t) - ho]}{ho} \text{ being } \frac{d\varepsilon}{dt} = \frac{V_{deb}}{h_o} \quad (2)$$

Figure 5 shows the stress-strain curves for tack tests with initial gaps of 0.5 and 0.1 mm, respectively. As can be seen, the higher the HMDI content in the composition the higher the adhesive strength in

the sample. Basically, the viscoelastic adhesion increases with the amount of urethane bonds present in the adhesive. The peculiar shape of the curve (initial small increase in stress followed by a plateau region and an extra increase in the stress) typically represents a fibrillation process in the adhesive. Basically, when one of the surface (glued by adhesive) moved away with certain debonding speed (V_d), the physical separation of adhesive starts to form elongated structures of polymeric chains, which appeared as fibres. This phenomenon is generally called as a fibrillation process. Moreover, the area under the curve gives access to the adhesion energy (E_{ad}) which can be calculated as follows (Fernández et al., 2010):

$$E_{ad} = h_o \int_0^{\epsilon_{max}} \sigma(\epsilon) d\epsilon \quad (3)$$

E_{ad} increases with the HMDI content at constant debonding velocity and is highest for sample CO-75 (see Table 2A and 2B). Interestingly, the same adhesives when tested in tack experiments with an initial lower gap of 0.1 mm exhibited a dramatic increase in the adhesion energy when compared with the same debonding speed at the higher initial gap of 0.5 mm. Thus, all the samples have the highest adhesive strength at 0.1 mm initial gap and debonding speed of 5 mm/s. It is worthy to remark that not only the debonding speed but also the initial gap significantly influences the E_{ad} in the probe tack measurements and therefore exert an important role in controlling the adhesion strength, sometimes even determining the predominant adhesion mechanism. Basically, the adhesives with low strain rate ($\leq 5\ s^{-1}$) exhibit more viscous adhesion behaviour and those with higher strain rate ($\geq 5\ s^{-1}$) show a stronger viscoelastic adhesion (fibrillation) (Fernández et al., 2010). Obviously, the internal microstructure of these adhesives, which is determined by the type and amount of chemical bonding, also plays an important role in controlling the deformability of the network, hardening, and tackiness observed in rheological and tack experiments.

3.5 Surface Morphology of Adhesives

For a better understanding of the structure-property relationships, the adhesives microstructure was investigated by SEM. Figure 6 shows the microstructure of CO-86 and CO-75, at different level of

magnification. Basically, the adhesive with lower amount of crosslinker (CO-86) shows an interconnected fibre-like structure, whereas the adhesive with the highest amount of HMDI shows a densely-packed structure yielding a stronger interconnecting network. The observation of these morphologies supports the analysis made from rheological and tack tests regarding the viscoelastic adhesion mechanisms, which occurred due to the presence of fibre-like structures. However, it is well known that cross-linked gel systems can be structured at different levels of organization. Thus, for instance, the network mesh which results from the crosslinked structures can present sufficient mobility to rearrange into larger fibrils for gelatin-based hydrogels (Marmorat et al., 2016). This was basically observed for the systems with the lower amount of crosslinker which is expected to form a network with lower crosslinking density, i.e. larger spacing among cross-linking points.

3.6 Small Angle X-Ray Scattering measurements

To elucidate the effect of the network mesh size at the nanoscale, SAXS measurements were consequently performed to detail the nanostructure of these adhesives. The scattering patterns obtained from CO adhesives were modelled assuming that the scattering intensity arises from two q dependent contributions, similar to that previously described by Debye and Bueche (Debye and Bueche, 1949; Domingues et al., 2013).

$$I(q) = I_{Excess}(q) + I_{Network}(q) + bkg \quad (4)$$

The first contribution is typically referred to as the excess scattering term and takes into account low-q scattering from the presence of inhomogeneities in the system (i.e. cross-linking points, solid-like polymer domains) (Shibayama, 1998). Here, the excess term is modelled by a Guinier function describing a phase characterised by a radius of gyration (Shibayama et al., 1992).

$$I_{Exccess}(q) = I_G(0) exp\left(\frac{-q^2 R_g^2}{3}\right) \quad (5)$$

where, $I_G(0)$ is the Guinier excess intensity at q = 0 and R_g is the radius of gyration of the inhomogeneity.

The second term accounts for scattering coming from the presence of a 3D network characterised by a

correlation length that describes the so-called "blob" size as seen in semi-dilute polymer and gel systems. This is given by (Hammouda et al., 2004):

$$I_{Network}(q) = \frac{I_L(0)}{1+(Q\xi)^n} \quad (6)$$

where, $I_L(0)$ is the network scattering intensity at q = 0 and ξ the correlation length describing the blob size. The fractal dimension (*n*) is 2 for pure semi-dilute polymer systems and gels which have overlapping polymer chains and increases towards 4 for systems where the scattering is more solid-particle like with two phases sharply defined by an interface. The experimental data and fits to the model described in equations 4-6 are shown in Figure 7 and fitting parameters presented in Table 3. In the fitting procedure, the n factor was varied in the range of 2.5–3.2 and was subsequently fixed to the average value of 2.8. This is indicative of a system where the polymer chains are slightly collapsed and somewhere between a semi-dilute system (n=2) and a fully collapsed system describing solid-like particles (n=4). From the fitting parameters, it is evident that as the cross-linking density increases i.e. more urethane bonds are present; the correlation lengths decrease. This is as expected as in the classic description of a cross-linked, semi-dilute polymer gel, the blob size formed by the polymer coils is comparable to the distance between the cross-linking points which in turn is commensurate with the mesh size (Scherer, 1994; Weber et al., 2009). On the other hand, the domain size of the inhomogeneity is shown to be independent on the degree of crosslinking at the –NCO/–OH mole ratios studied. $I_G(0)/I_L(0)$ ratio is proportional to the density of inhomogeneity with respect to the polymer network, as the HDMI is increased in the adhesive this quantity increases (see last column of Table 3) proving that the inhomogenieties are mostly associated to the inhomogeneity in the crosslinking points. The correlation length (*ξ*) decreases (from 29 to 14 Å) with the increase in CO/HMDI weight ratio (from 1:0.032 to 1:0.32). Interdependency of CO/HMDI weight ratio, elastic modulus, and correlation length, resulted into two simple mathematical relationships. Both adhesion energy (E_{ad}) and storage modulus (G') versus correlation length (*Å*) can be modelled by using a power law equation as given below.

$$E_{ad} = a\,\xi^{-P1} \quad \text{and} \quad G' = b\,\xi^{-P2} \quad (7a \text{ and } 7b)$$

It could be seen clearly in Figure 8A and 8B that with decreasing the correlation length from 29 to 14 *Å*, storage modulus and E_{ad} increases. This is a coherent conception as with an increase in crosslinking density, the number of net-points is increased and the blob size decreases which results in a simultaneous enhancement of the elasticity/rigidity of the system. A reciprocal relationship between the storage modulus, G', and mesh size is expected from the standard rubber elasticity theory (Marmorat et al., 2016). Similar discussion holds for the relationship between correlation length and adhesion energy. In this case, it is worthy to notice that the value of the power-law exponent, P1 (shown in Table S2 in ESI) seems to be mainly dependent on the initial gap, being around 1.8-2 for 0.1 mm and 3.7-3.8 for 0.5 mm, and not so on the resulting strain rate. Regarding these evidences, a more in deep investigation is needed to elucidate the role of the extensional rheological properties in the adhesion mechanisms. Moreover, as shown in Figure S1B (ESI), adhesives resulted from this study show a wide range of tenability and can adherer to different surfaces as, wood and metal.

4. Conclusions

This study demonstrates a simple way of preparation of volatile solvent-free adhesives under mild reaction conditions. The adhesives were cured at room conditions without any external treatments like heat or irradiation of light. The mechanical properties and microstructure of the adhesives can be controlled by the amount of HMDI in the composition. The lower thermal stability of the adhesive systems was related to the presence of polyurethane linkages, which favour a faster degradation compared to pure castor oil. Further, it was deduced from SEM and SAXS analysis that the increase in HMDI concentration significantly changes the microstructure of these adhesives. More compact structures with lower correlation lengths are formed due to additional crosslinking points in the network, thus yielding higher values of the linear viscoelastic functions and adhesiveness. The rheological behaviour of the adhesives (i.e. the elastic modulus, adhesiveness and the adhesion energy), can be simply tuned by changing the monomer to crosslinker ratio, i.e. the input isocyanate

index. Moreover, interdependencies between the storage modulus, adhesion energy, and correlation length support the strong relationship between mechanical/functional properties and the micro-structure of these adhesives. All the presented results show that it is possible to easily tune the viscoelastic properties, microstructure and performances of these castor oil based adhesives by simply controlling the amount of HMDI thus paving the way to a wide variety of new applications in the area of solvent free biodegradable sustainable adhesives.

Acknowledgements

This work is a part of research project ISSFLOW (Project ID: 612330) sponsored by European Union under the program FP7-PEOPLE. The authors also acknowledge partial financial support from the Consorzio per lo sviluppo dei Sistemi a Grande Interfase (CSGI).

References

Borrero-López, A.M., Valencia, C., Franco, J.M., 2017. Rheology of lignin-based chemical oleogels prepared using diisocyanate crosslinkers: Effect of the diisocyanate and curing kinetics. Eur. Polym. J. 89, 311–323. https://doi.org/10.1016/j.eurpolymj.2017.02.020

Debye, P., Bueche, A.M., 1949. Scattering by an inhomogeneous solid. J. Appl. Phys. 20, 518–525. https://doi.org/10.1063/1.1698419

Domingues, J.A.L., Bonelli, N., Giorgi, R., Fratini, E., Gorel, F., Baglioni, P., 2013. Innovative hydrogels based on semi-interpenetrating p(HEMA)/PVP networks for the cleaning of water-sensitive cultural heritage artifacts. Langmuir 29, 2746–2755. https://doi.org/10.1021/la3048664

Donnelly, M.J., Stanford, J.L., Still, R.H., 1991. The conversion of polysaccharides into polyurethanes: A review. Carbohydr. Polym. 14, 221–240. https://doi.org/10.1016/0144-8617(91)90078-Q

Ebnesajjad, S., Landrock, A.H., 2015. Adhesive Applications and Bonding Processes, in: Adhesives Technology Handbook. Elsevier, pp. 206–234. https://doi.org/10.1016/B978-0-323-35595-7.00008-5

Engels, H.W., Pirkl, H.G., Albers, R., Albach, R.W., Krause, J., Hoffmann, A., Casselmann, H., Dormish, J., 2013. Polyurethanes: Versatile materials and sustainable problem solvers for today's challenges. Angew.

Chemie - Int. Ed. 52, 9422–9441. https://doi.org/10.1002/anie.201302766

Fernández, M., Landa, M., Muñoz, M.E., Santamaría, A., 2010. Tackiness of an electrically conducting polyurethanenanotube nanocomposite. Int. J. Adhes. Adhes. 30, 609–614. https://doi.org/10.1016/j.ijadhadh.2010.05.011

Frisch, K.C., 2002. Chapter 16 – Chemistry and technology of polyurethane adhesives, in: Adhesion Science and Engineering. Elsevier, pp. 759–812. https://doi.org/10.1016/B978-044451140-9/50016-0

Gallego, R., Arteaga, J.F., Valencia, C., Franco, J.M., 2015. Thickening properties of several NCO-functionalized cellulose derivatives in castor oil. Chem. Eng. Sci. 134, 260–268. https://doi.org/10.1016/j.ces.2015.05.007

Gallego, R., González, M., Arteaga, J.F., Valencia, C., Franco, J.M., 2014. Influence of functionalization degree on the rheological properties of isocyanate-functionalized chitin- and chitosan-based chemical oleogels for lubricant applications. Polymers (Basel). 6, 1929–1947. https://doi.org/10.3390/polym6071929

Gurunathan, T., Mohanty, S., Nayak, S.K., 2015. Isocyanate terminated castor oil-based polyurethane prepolymer: Synthesis and characterization. Prog. Org. Coatings 80, 39–48. https://doi.org/10.1016/j.porgcoat.2014.11.017

Hammouda, B., Ho, D.L., Kline, S., 2004. Insight into clustering in poly(ethylene oxide) solutions. Macromolecules 37, 6932–6937. https://doi.org/10.1021/ma049623d

Howard, G.T., 2002. Biodegradation of polyurethane: A review. Int. Biodeterior. Biodegrad. 49, 245–252. https://doi.org/10.1016/S0964-8305(02)00051-3

Lambuth, A.L., 1989. Adhesives from Renewable Resources, in: Adhesives from Renewable Resources. pp. 1–10. https://doi.org/10.1021/bk-1989-0385.ch001

Marmorat, C., Arinstein, A., Koifman, N., Talmon, Y., Zussman, E., Rafailovich, M., 2016. Cryo-Imaging of Hydrogels Supermolecular Structure. Sci. Rep. 6, 25495. https://doi.org/10.1038/srep25495

Mythili, C. V., Retna, A.M., Gopalakrishnan, S., 2004. Synthesis, mechanical, thermal and chemical properties of polyurethanes based on cardanol. Bull. Mater. Sci. 27, 235–241. https://doi.org/10.1007/BF02708512

Raftery, T., Gilles, R., 1995. JCPDS-International Centre for Diffraction Data Round Robin Study of Silver Behenate. A Possible Low-Angle X-Ray Diffraction Calibration Standard. Powder Diffr. 10, 91–95. https://doi.org/10.1017/S0885715600014421

Ratajska, M., Boryniec, S., 1998. Physical and chemical aspects of biodegradation of natural polymers. React.

Funct. Polym. 38, 35–49. https://doi.org/10.1016/S1381-5148(98)00031-5

Scherer, G.W., 1994. Hydraulic radius and mesh size of gels. J. Sol-Gel Sci. Technol. 1, 285–291. https://doi.org/10.1007/BF00486171

Shibayama, M., 1998. Spatial inhomogeneity and dynamic fluctuations of polymer gels. Macromol. Chem. Phys. 199, 1–30. https://doi.org/10.1002/macp.1998.021990101

Shibayama, M., Tanaka, T., Han, C.C., 1992. Small angle neutron scattering study on poly(N-isopropyl acrylamide) gels near their volume-phase transition temperature. J. Chem. Phys. 97, 6829–6841. https://doi.org/10.1063/1.463636

Silva, B.B.R., Santana, R.M.C., Forte, M.M.C., 2010. A solventless castor oil-based PU adhesive for wood and foam substrates. Int. J. Adhes. Adhes. 30, 559–565. https://doi.org/10.1016/j.ijadhadh.2010.07.001

Simon, J., Barla, F., Kelemen-Haller, A., Farkas, F., Kraxner, M., 1988. Thermal stability of polyurethanes. Chromatographia 25, 99–106. https://doi.org/10.1007/BF02259024

Somani, K., Kansara, S., Parmar, R., Patel, N., 2004. High solids polyurethane coatings from castor-oil-based polyester-polyols. Int. J. Polym. Mater. Polym. Biomater. 53, 283–293. https://doi.org/10.1080/00914030490267618

Somani, K.P., Kansara, S.S., Patel, N.K., Rakshit, A.K., 2003. Castor oil based polyurethane adhesives for wood-to-wood bonding. Int. J. Adhes. Adhes. 23, 269–275. https://doi.org/10.1016/S0143-7496(03)00044-7

Tenorio-Alfonso, A., Pizarro, M.L., Sánchez, M.C., Franco, J.M., 2018. Assessing the rheological properties and adhesion performance on different substrates of a novel green polyurethane based on castor oil and cellulose acetate: A comparison with commercial adhesives. Int. J. Adhes. Adhes. 82, 21–26. https://doi.org/10.1016/j.ijadhadh.2017.12.012

Verdier, C., Piau, J.-M., 2003. Effect of nonlinear viscoelastic properties on tack. J. Polym. Sci. Part B Polym. Phys. 41, 3139–3149. https://doi.org/10.1002/polb.10470

Weber, L.M., Lopez, C.G., Anseth, K.S., 2009. Effects of PEG hydrogel crosslinking density on protein diffusion and encapsulated islet survival and function. J. Biomed. Mater. Res. Part A 90A, 720–729. https://doi.org/10.1002/jbm.a.32134

Zhang, C., Madbouly, S.A., Kessler, M.R., 2015. Biobased polyurethanes prepared from different vegetable oils. ACS Appl. Mater. Interfaces 7, 1226–1233. https://doi.org/10.1021/am5071333

Zuber, M., Zia, F., Zia, K.M., Tabasum, S., Salman, M., Sultan, N., 2015. Collagen based polyurethanes—A review of recent advances and perspective. Int. J. Biol. Macromol. 80, 366–374. https://doi.org/10.1016/j.ijbiomac.2015.07.001

Figures and Tables:

Table 1. Composition of CO-HMDI adhesives

Composition		Nomenclature	CO/HMDI weight ratio	Isocyanate index (–NCO/-OH mole ratio)*	Yield (wt%)
CO (g)	HMDI (g)				
96.88	3.12	CO-97	1:0.032	0.14	95
95.40	4.60	CO-95	1:0.048	0.21	96
92.55	7.45	CO-92	1:0.081	0.36	97
86.15	13.85	CO-86	1:0.161	0.71	96
75.66	24.34	CO-75	1:0.321	1.43	96

* according to the CO fatty acid profile reported in Quinchia et al., (2010), i.e. 82.5%ricinoleic acid

Table 2A. Summary of probe-tack test: maximum stress σ_s, adhesion energy E_{ad}, and Strain at failure ε_f determined from the strain-strain results of Figure 5 and 6 at V_d = 1 mm/s

Samples	V_d = 1 mm/s (at gap = 0.5 mm)			V_d = 1 mm/s (at gap = 0.1 mm)		
	σ_s (Pa)	E_{ad} (J/m^2)	ε_f	σ_s	E_{ad} (J/m^2)	ε_f
CO-97	0.12 x 10^4	0.56	1	1.2 x 10^4	3.6	6.6
CO-95	0.43x 10^4	1.3	1.3	2.27 x 10^4	7.1	6.6
CO-92	0.43 x 10^4	1.6	1.6	2.9 x 10^4	8.5	7.9
CO-86	1.7 x 10^4	9.5	2.2	3.4 x 10^4	14.9	9.8
CO-75	1.6 x 10^4	11.3	2.2	4.2 x 10^4	17.7	10.5

Table 2B. Summary of probe-tack test: maximum stress σ_s, adhesion energy E_{ad}, and Strain at failure ε_f determined from Figures 5 and 6 at V_d = 5 mm/s.

Samples	V_d = 5 mm/s (at gap = 0.5 mm)			V_d = 5 mm/s (at gap = 0.1 mm)		
	σ_s (Pa)	E_{ad} (J/m^2)	ε_f	σ_s	E_{ad} (J/m^2)	ε_f
CO-97	0.28 x 10^4	1.6	2.1	2.25 x 10^4	8.5	9.5
CO-95	0.65 x 10^4	3.6	2.3	2.46 x 10^4	8.4	9.2
CO-92	1.6 x 10^4	6.7	2.6	3.6 x 10^4	13.6	10.4
CO-86	2.5 x 10^4	16.6	3.0	4.2 x 10^4	26.9	15.9
CO-75	2.7 x 10^4	32.9	3.8	5.8 x 10^4	36.8	18.5

Table 3. Parameters obtained from fitting CO/HMDI data to equation 2 – 4.

Samples	Fit parameters					
	$I_G(0)$	R_g / $\pm$ 5 Å	$I_L(0)$	ξ / $\pm$ 0.5 Å	n	$I_G(0)/I_0(0)$
CO-97	100	140	31.0	29	2.8	3.2
CO-95	110	135	26.0	28	2.8	4.2
CO-92	76	142	12.8	25	2.8	5.9
CO-86	22.5	139	14.3	16	2.8	1.6
CO-75	40.6	138	5.1	14	2.8	7.9

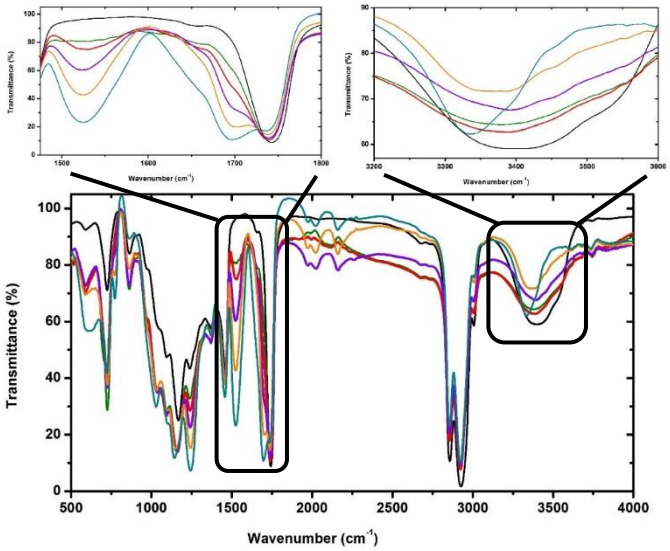

Figure 1. ART-FTIR spectra of CO (—), CO-97 (—), CO-95 (—), CO-92 (—), CO-86 (—), and CO-75 (—). The urethane bond formation can be seen by the absorption peak at: 1530-1545 cm^{-1} due to the H-N-C=O amide II vibrations, 1690-1700 cm^{-1} due to –C=O stretching vibrations in urethane and 3360-3380 cm^{-1} due to –N-H stretching.

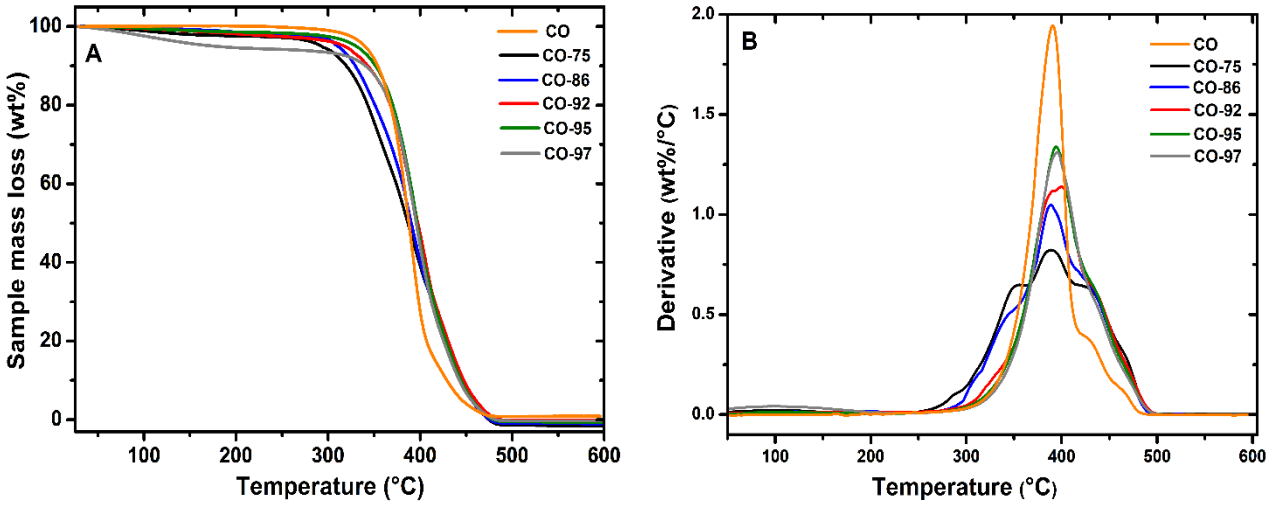

Figure 2. Thermogravimetric analysis of CO (—), CO-97 (—), CO-95 (—), CO-92 (—), CO-86 (—), and CO-75 (—) representing (A) sample mass loss (wt%) versus temperature and (B) derivative thermograms versus temperature.

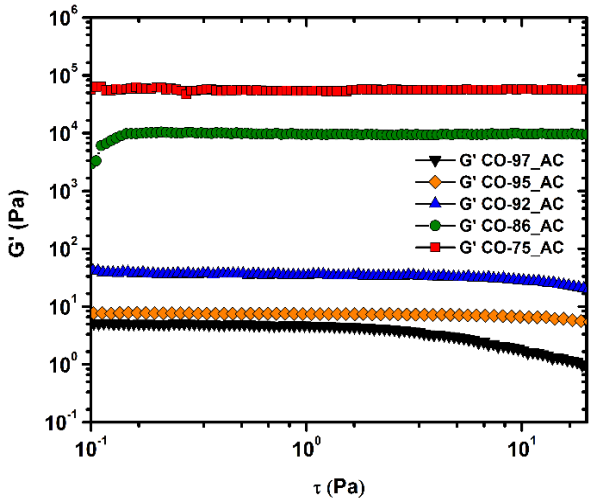

Figure 3. Stress controlled amplitude sweep of CO-97, CO-95, CO-92, CO-86, and CO-75 after cuing (AC) at room temperature (25 °C and f = 0.5 Hz).

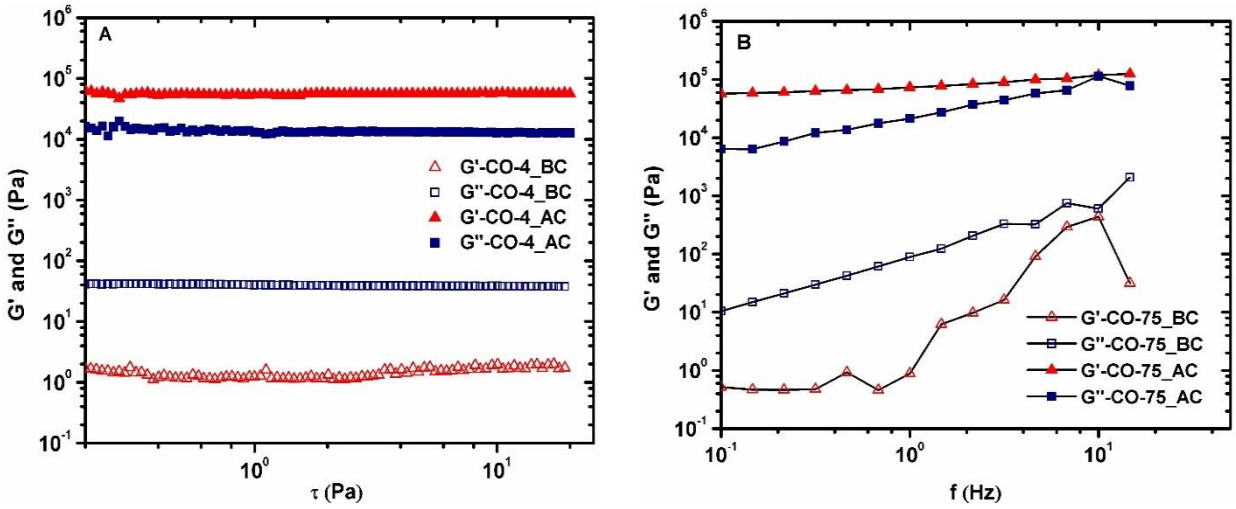

Figure 4. Rheological measurements of CO-75, A) Stress controlled amplitude sweep of CO-75 before curing (BC) and after cuing (AC) at room temperature (25 °C and f = 0.5 Hz) and B) Storage modulus, *G′*, and loss modulus, *G″*, as a function of frequency for CO-75 before curing (BC) and after curing (AC) at room temperature (25 °C).

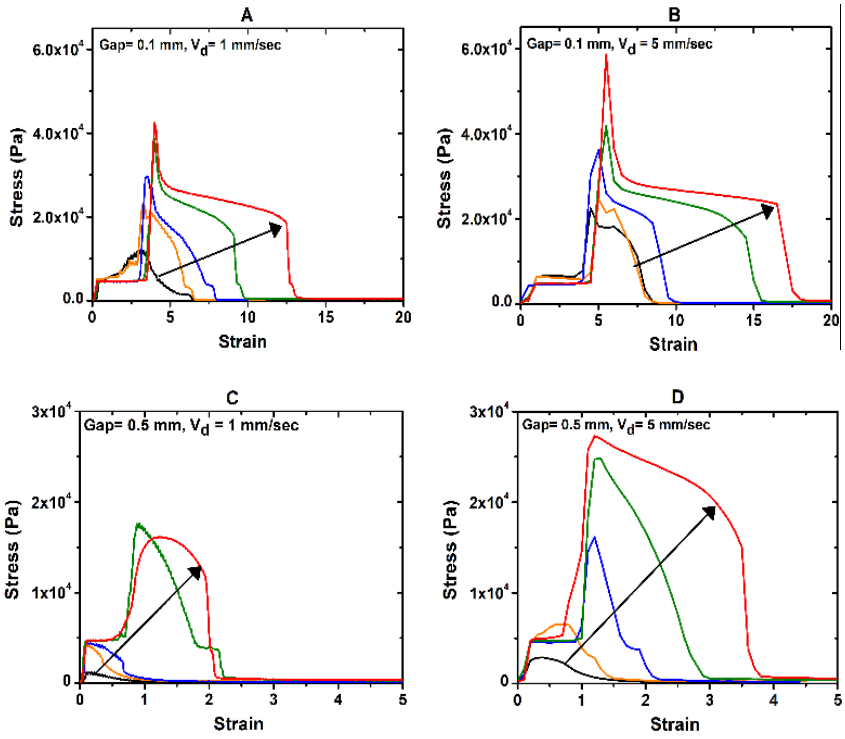

Figure 5. Tack test of adhesives CO-97 (—), CO-95 (—), CO-92 (—), CO-86 (—), and CO-75 (—). A) Gap = 0.1 mm and V_d= 1 mm/sec. B) Gap = 0.1 mm and V_d= 5 mm/sec. C) Gap = 0.5 mm and V_d= 1 mm/sec. D) Gap = 0.5 mm and V_d= 5 mm/sec.

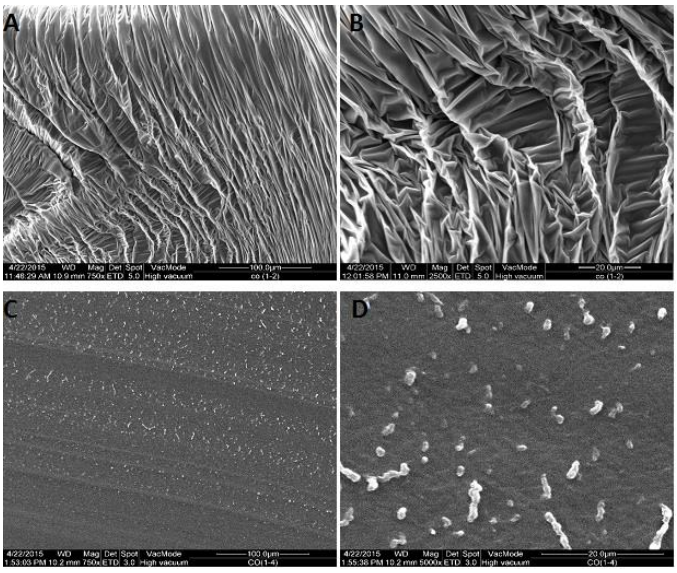

Figure 6. SEM images of adhesive CO-86 at different magnification A) 750X and B) 2500X. CO-75 at different magnification of C) 750X and D) 5000X. The fibre-like structure (CO-86) and densely packed structure (CO-75) highlight the structural changes due to different degree of crosslinking.

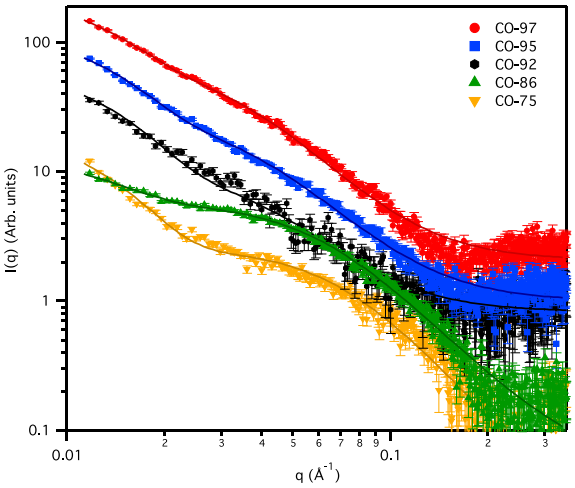

Figure 7. Log-log representation of the SAXS intensity profiles from CO-97 (red circles), CO-95 (blue squares), CO-92 (black hexagons), CO-86 (green triangles) and CO-75 (downward facing yellow triangles). Solid lines show fits to model described in equations 2-4.

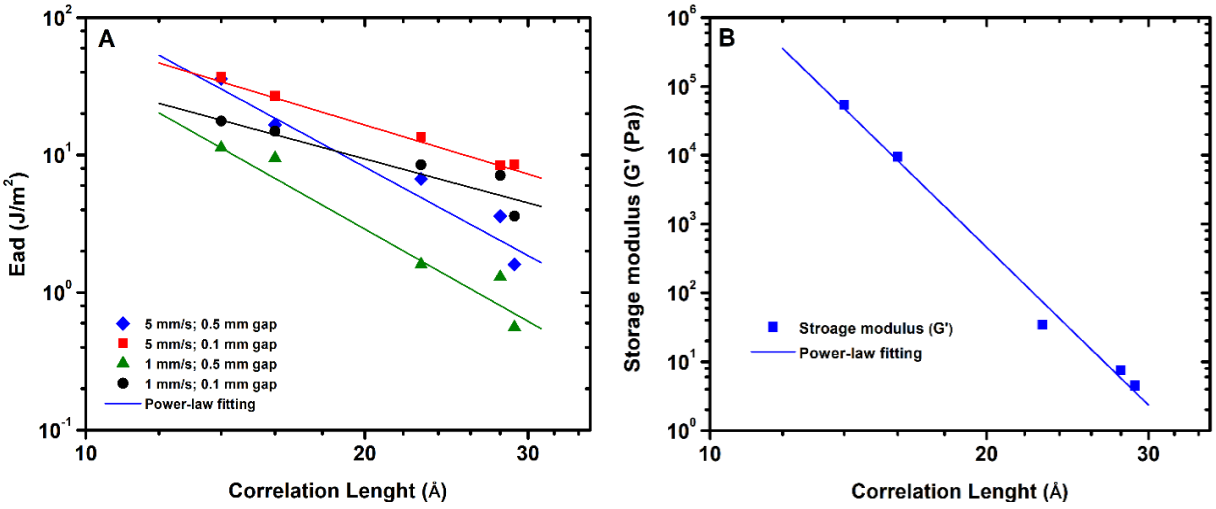

Figure 8. Correlation between A) adhesion energy (E_{ad} (J/m^2)) and correlation length (*Å*), and B) storage modulus (*G'*) and correlation length (*Å*). Parameters describing the fitting lines according to equation 7a (panel A) are reported in Table S2 while the parameters obtained from equation 7b (panel B) are b=4x10^{19} (J/ Å^{P2} m^2) and $P2$=-13.